scientific reports

Check for updates

OPEN

Antibiofilm activity of ZnO–Ag nanoparticles against *Pseudomonas aeruginosa*

Fatima Alhosani[1,8], Deema Islayem[2,6,8], Shamma Almansoori[2], Awais Zaka[3,5], Laith Nayfeh[1], Ayman Rezk[2,5], Ahmed F. Yousef[4,6,7], Anna Maria Pappa[2] & Ammar Nayfeh[1,5]✉

Biofilm-related infections remain a major concern in clinical settings due to the increasing challenge of antimicrobial resistance to conventional antimicrobial treatments. Surface coatings of nanomaterials that can effectively prevent biofilm formation and disrupt established biofilms are essential to addressing this challenge. In this study, a ZnO–Ag nanocomposite was synthesized via a dry chemical method and characterized using XRD, XPS, TEM, SEM-EDX, and AFM, confirming the presence of highly crystalline and pure ZnO and Ag nanoparticles with sharp nanoscale features. The nanocomposite demonstrated potent antibiofilm activity against *Pseudomonas aeruginosa*, a common Gram-negative biofilm-forming pathogen. Surface-coated glass slides prevented initial biofilm formation, while treatment with higher nanocomposite concentrations (≥ 0.25 g/L) significantly disrupted pre-formed biofilms and altered biofilm architecture, as shown by SEM and crystal violet assays. Mechanistic investigations suggested that nanoparticle surface sharpness may contribute to membrane disruption, and EPR analysis confirmed the generation of reactive oxygen species (ROS), particularly superoxide and methyl radicals, under light exposure. These results highlight the composite's strong potential for integration into surfaces prone to bacterial colonization, offering a practical approach for reducing biofilm-related complications.

Bacterial infection is a major global health concern posing significant challenges to healthcare systems due to their high morbidity, mortality rates, and the increasing prevalence of antibiotic resistance[1]. The majority of bacterial infections are associated with biofilms, which are structured microbial communities that adhere to surfaces and are embedded within a self-produced extracellular polymeric substance (EPS)[2]. EPS matrix allows biofilms to survive under harsh conditions and acts as a protective barrier against external threats such as antibiotics, by limiting their penetration and reducing their effectiveness[3]. Biofilms are significantly more resistant to antibiotics compared to planktonic bacteria[4]. As a result, conventional antibiotic therapies often fail to eradicate biofilms, leading to persistent and recurrent infections, particularly in clinical settings such as catheter-associated urinary tract infections, implant-related infections, and chronic wounds[5]. Furthermore, the misuse, overuse, and prolonged use of antibiotics to treat biofilm-associated infections have accelerated the emergence of antibiotic-resistant bacteria, which is now recognized as one of the greatest threats to global health[6]. Therefore, there is an urgent need for the development of novel and effective treatments to combat biofilm-related infections. Recently, advancements in nanotechnology, specifically nanomaterials, have led to the development of novel antimicrobial agents that have greater activity against various types of bacterial cells compared to traditional antibiotics[7]. The synthesis methods used to produce these nanomaterials play a crucial role in determining their physiochemical properties, such as size, shape, and surface chemistry, which can be precisely controlled to optimize their interaction with bacterial cells[8,9]. Additionally, many metal nanomaterials in nature possess intrinsic antibacterial activity and can act as delivery vehicles, transporting antibiotics or other antimicrobial agents directly to bacterial cells, including those within biofilms, thus overcoming barriers to treatment[10]. Among the most extensively studied nanomaterials for antibacterial purposes are silver (Ag) and zinc oxide (ZnO). Ag is commonly used in ointments and wound dressings, and food packaging to prevent

[1]Department of Electrical Engineering, Khalifa University, Abu Dhabi, United Arab Emirates. [2]Department of Biomedical Engineering, Khalifa University, Abu Dhabi, United Arab Emirates. [3]Department of Chemical Engineering, Khalifa University, Abu Dhabi, United Arab Emirates. [4]Department of Biological Sciences, Khalifa University, Abu Dhabi, United Arab Emirates. [5]Research and Innovation Center for Graphene and 2D Materials (RIC-2D), Khalifa University, Abu Dhabi, United Arab Emirates. [6]Biotechnology Center (BTC), Khalifa University, Abu Dhabi, United Arab Emirates. [7]Center for Membranes and Advanced Water Technology (CMAT), Khalifa University, Abu Dhabi, United Arab Emirates. [8]Fatima Alhosani, Deema Islayem have contributed equally to this work. ✉email: Ammar.nayfeh@ku.ac.ae

contamination[11,12]. On the other hand, ZnO is used in additive pharmaceutical drugs formulations, sanitizers, cosmetics and food packaging. Both Ag and ZnO exhibit antibacterial activity by the generation of reactive oxygen species (ROS), leading to oxidative stress thereby damaging the bacterial cell membranes, proteins, and DNA[13]. The oxidative damage increases the membrane permeability, ultimately causing cell lysis[14,15]. Additionally, silver (Ag^{+}) and zinc ions (Zn^{2+}), released from their respective materials, further disrupt bacterial membranes and interfere with essential enzymatic processes and metabolic pathways[16,17]. They also bind to bacterial DNA, impairing replication, transcription, and protein synthesis[18]. Building upon their antibacterial properties, many studies have reported that Ag and ZnO NPs exhibit antibiofilm activities influenced by factors such as particle size, concentration, surface charge, and the specific bacterial species involved, making them effective against biofilm-associated infections[19–22]. For example, it has been proposed that surfaces coated with Zn or Ag prevent initial bacterial adhesion through interfering with quorum sensing; the bacterial communication system that regulates biofilm formation, thereby reducing the production of virulence factors and hindering the establishment of biofilms[23,24]. Moreover, sublethal Zn or Ag concentrations could affect biofilm formation by disrupting amyloid fibril formation, which is essential for biofilm structural integrity[25]. For example, they can interfere with the assembly of amyloid proteins like FapC in *Pseudomonas aeruginosa*, thereby hindering biofilm development and stability and weakening the biofilm matrix, thus enhancing bacterial susceptibility to antimicrobial treatments[26]. Combining Ag and ZnO into a single nanocomposite creates a synergistic effect, significantly enhancing their antibacterial effect. Ag has been reported to be stronger than ZnO alone against micro-organisms[27], but this comes at the cost of a higher toxicity[28]. To reduce that toxicity, and enhance the biocompatibility, ZnO is doped with Ag to create a material that has antibacterial activity with lower toxicity[29,30]. A majority of studies on ZnO–Ag nanocomposites have focused on evaluating their antibacterial properties, particularly against planktonic cultures of bacteria. However, such methods may not accurately reflect surface efficacy in biofilm applications where infections present a far more significant challenge due to the resilience and complexity of biofilms. While a few studies have investigated the antibiofilm activity of ZnO–Ag nanocomposites, most have concentrated on only one aspect, either the prevention of biofilm formation, or the disruption of pre-formed biofilms[31–34]. These studies have been conducted on various bacterial species, but to date, very few have addressed *Pseudomonas aeruginosa*, a key pathogen known for its biofilm formation in clinical settings. Among the limited studies on *P. aeruginosa*, one focused primarily on the indirect antibiofilm effects, such as quorum sensing and virulence factors inhibition[35], rather than assessing the direct structural and behavioral changes in biofilms. In contrast, our study provides a more comprehensive evaluation of a simple and scalable ZnO–Ag nanocomposite by examining both its preventive and disruptive effects on *P. aeruginosa* biofilms in a concentration-dependent manner. This direct approach allows us to assess both biofilm formation and disruption, offering insights into the nanocomposite's optimal usage and the ability to both prevent and treat biofilm-related infections. Furthermore, unlike some earlier studies that employed more complex or polymer-based composite systems (e.g., chitosan coatings, zeolite matrices)[36,37], the synthesis method used in our work is straightforward, scalable, and matrix-free, potentially offering enhanced translational value in real-world applications.

Experimental methods

Materials and instrumentation

To synthesize the ZnO–Ag nanocomposite, Zinc Acetate Dihydrate (98%) from Sigma-Aldrich and Silver Nitrate (99.9995%) from Alfa Aesar GmbH were mixed and synthesized using a dry chemical method. The composition of the material was characterized by X-ray diffraction (XRD, PANalytical Empyrean) for the crystalline structure, X-ray photoelectron spectroscopy (XPS, Escalab Xi+) for binding energies, and scanning electron microscopy (SEM, FEI Quanta 250 FEG-ESEM) and transmission electron microscopy (TEM, FEI Tecnai TEM 200 kV) for imaging and energy dispersive X-ray (EDX) analysis. To analyze the material's surface morphology, 500 µL of the nanocomposite suspension at a concentration of 5 mg/mL was spin-coated with a speed of 500 rpm for 60 s on a 1 cm × 1 cm glass slide. Atomic force microscopy (AFM, MFP-3D Origin AFM) in air tomography mode was performed to reveal insights into the surface morphology of the material, as one of the reported antibacterial mechanisms of ZnO in the literature is the presence of sharp edges[38]. Electron paramagnetic resonance (EPR) was used to detect radicals, a key antibacterial mechanism. 11.8 mg of DMPO was dissolved in 1 mL of methanol, followed by 1 mg of the nanocomposite and 5 min of sonication. 200 µL of the mixture was transferred into an EPR glass tube, and EPR measurements were performed using a Bruker EMX Nano system under both light-irradiated (10 min) and non-irradiated conditions, with microwave attenuation set at 50.

Synthesis of ZnO–Ag NPs and glass slide coating

ZnO–Ag NPs were synthesized using a simple calcination-impregnation method adopted from[39] by initially dissolving Zinc Acetate Dihydrate and Silver Nitrate in deionized water at a 2:1 ratio. The mixture was stirred for 5 min at 500 rpm and then sonicated for 5 min, producing a solid precursor. This precursor was then placed in a muffle furnace and calcined at 400 °C for 1 h. During the calcination process, the zinc acetate decomposed to form zinc oxide, whereas the silver nitrate decomposed to produce silver nanoparticles. The resultant ZnO–Ag composite, which had a milky brown color, was allowed to cool to room temperature before suspension in DI water and probe sonication for 10 min (5 s on, 5 s off, 50% amplitude). Glass slides were spin-coated with the suspension at 600 rpm for 1 min, before being placed on a 100 °C hot plate for 1 h to evaporate the solvent.

Bacterial strain and growth condition

Pseudomonas aeruginosa (ATCC 156922) was initially revived from a glycerol stock by streaking it onto an LB agar plate, which was then incubated at 37 °C for 24 h. Single colonies were selected and transferred into LB broth, where they were grown in a shaker incubator at 120 rpm and 37 °C for 24 h. After this incubation period, the culture's optical density (OD) at 600 nm was measured using a spectrophotometer. The bacterial culture was

then diluted with fresh LB broth to an OD of 0.2 in order to stimulate cells to enter the exponential growth phase for subsequent experiments.

Antibiofilm properties of ZnO–Ag nanocomposite

To evaluate the material's antibacterial potential, an LB agar plate was inoculated with *P. aeruginosa*, and a small amount of the material solution was applied as a spot to the agar surface. After incubating the plate at 37 °C for 24 h, the inhibition zone surrounding the material was measured. *P. aeruginosa* was then cultured on coated glass slides for 3 days at 37 °C. Following the 3 days, samples were prepared for SEM by fixing them with 2% glutaraldehyde and dehydrating through a graded ethanol series (60%, 70%, 80%, 90%, and 100%). Following this, two complementary methods were employed to further evaluate the antibiofilm potential of ZnO–Ag nanocomposite.

First, the Congo red agar method was used to preliminarily test biofilm formation in the presence of different ZnO–Ag nanocomposite concentrations. Bacterial cultures were mixed with ZnO–Ag nanocomposite solutions at concentrations of 0.025 g/L, 0.125 g/L, 0.25 g/L, and 1.25 g/L and incubated in a shaker incubator at 37 °C for 2 h. The samples were then streaked onto Congo red agar plates and incubated at 37 °C for 24 h. The following day, plates were examined for colony color, which provided information on biofilm formation.

Second, *P. aeruginosa* biofilms were cultivated on 1 cm × 1 cm glass slides at 37 °C over 3 days. Various concentrations of ZnO–Ag nanocomposite suspension (0.025 g/L, 0.125 g/L, 0.25 g/L, and 1.25 g/L) were then applied to the established biofilms for 24 h. Following treatment with the ZnO–Ag nanocomposites, the biofilms were imaged using SEM as described earlier. For a quantitative assessment, biofilms were stained with crystal violet (CV) after first removing growth medium and gently washing with distilled water three times to eliminate planktonic bacteria. To stain the biofilms, 1 mL of 0.1% CV solution was applied to the biofilm following incubation at room temperature for 15 min. Excess CV solution was removed by gently washing three times with distilled water followed by drying at room temperature for 10 min. Biofilm bound CV dye was solubilized with 1 mL 95% ethanol and absorbance was measured at 500 nm using a spectrophotometer to quantify biofilm formation.

Results and discussion

Characterization of the material

The elemental composition and the crystalline phases were identified by performing X-ray diffraction (XRD) with a Cu anode material and Kα radiation of 1.54060 Å, with 2θ scans starting from 2 to 90° and a step size of 0.0260° per 56.8650 s. The peaks, shown in Fig. 1a, Ag, matched ICDD (04-004-8065), whereas ZnO peaks matched ICDD (01-086-8923). The X-ray diffraction (XRD) pattern of the ZnO–Ag nanocomposite exhibits distinct peaks at 2θ values of approximately 31.8°, 34.4°, 36.3°, and 38.1°, which correspond to the (100), (002), (101), and (111) planes of the hexagonal wurtzite structure of ZnO and the face-centered cubic structure of Ag. The sharpness and intensity of these peaks indicate high crystallinity of the synthesized nanocomposite. The peak at 38.1° is particularly indicative of the presence of metallic silver nanoparticles. The absence of any impurity peaks suggests the high purity of the synthesized ZnO–Ag nanocomposite. The narrow widths of the diffraction peaks imply that the nanocomposite consists of well-ordered crystallites with minimal internal strain.

Figure 1b shows the X-ray photoelectron spectroscopy (XPS) survey spectra of the ZnO–Ag nanocomposite, which shows the presence of all three elements present: Ag, ZnO, and O. The O 1s peak in Fig. 1c is asymmetric, hence it needs to be separated into two symmetrical peaks, with the peak at 532.6 eV indicating the presence of a metal hydroxyl at the surface and the peak at 531 eV indicating the presence of oxygen combined with a metal, specifically ZnO[40,41]. Figure 1d depicts the high resolution Ag 3d spectrum. The binding energies of Ag $3d_{3/2}$ and Ag $3d_{5/2}$ are located at 374.2 eV and 368.2 eV, respectively, indicating that Ag is present in a metallic state. The high-resolution Zn 2p peaks are shown in Fig. 1e, where the binding energies of Zn $2p_{3/2}$ and Zn $2p_{1/2}$ are at 1022.3 eV and 1045.2 eV, respectively. The 22.9 eV difference indicates that Zn is present in a 2+ oxidation state.

The transmission electron microscopy (TEM) images of the ZnO–Ag nanocomposite reveal distinct morphological features, as shown in Fig. 2a. The particles exhibit a predominantly spherical shape with sizes ranging between 10 and 20 nm. Individual particles are well-resolved, with darker cores suggesting the presence of higher electron density regions, likely corresponding to silver nanoparticles. Aggregation is observed in some areas, as seen in the middle and right images, indicating potential interactions between the Ag and ZnO components or partial agglomeration during synthesis. To confirm the chemical composition of the material, an energy-dispersive X-ray (EDX) mapping was performed on the nanocomposite (attached to a carbon tape), as seen in Fig. 2b. EDX (Energy Dispersive X-ray Spectroscopy) is an analytical technique used to identify and quantify the elemental composition of a material by detecting the characteristic X-rays emitted from a sample when it is bombarded with high-energy electrons. An EDX area mapping was performed on Fig. 2c. Ag, Zn, O, and C (from carbon type) were detected. More specifically, Ag, Zn, and O were present in a 1:0.91:0.28 ratio. Based on the scanning electron microscopy (SEM) image, the surface appears rough and uneven, which is typical for nanocomposite materials, suggesting a high surface area that is beneficial for antibacterial applications.

One of the reported antibacterial mechanisms, reported in the literature, is the presence of sharp edges in ZnO, which physically disrupt the cell membrane of bacteria. A study conducted by Jeong et al.[38] demonstrated that the sharp edges of ZnO nanorods of different lengths ruptured the cell wall of *Escherichia coli*. To explore this mechanism of action, AFM in air tomography mode was used to investigate if the surface morphology of the material deposited on a glass slide, which is a surface biofilms typically grow on, showed sharp edges. As depicted in Fig. 3a, AFM scans of the material-coated glass slide revealed a rough surface with distinct peaks and valleys, where the height of the peaks varies and the maximum observed peak was 34 nm. Most of these peaks are sharp, indicating the presence of potential cutting edges that could disrupt bacterial cell membranes. The 2D

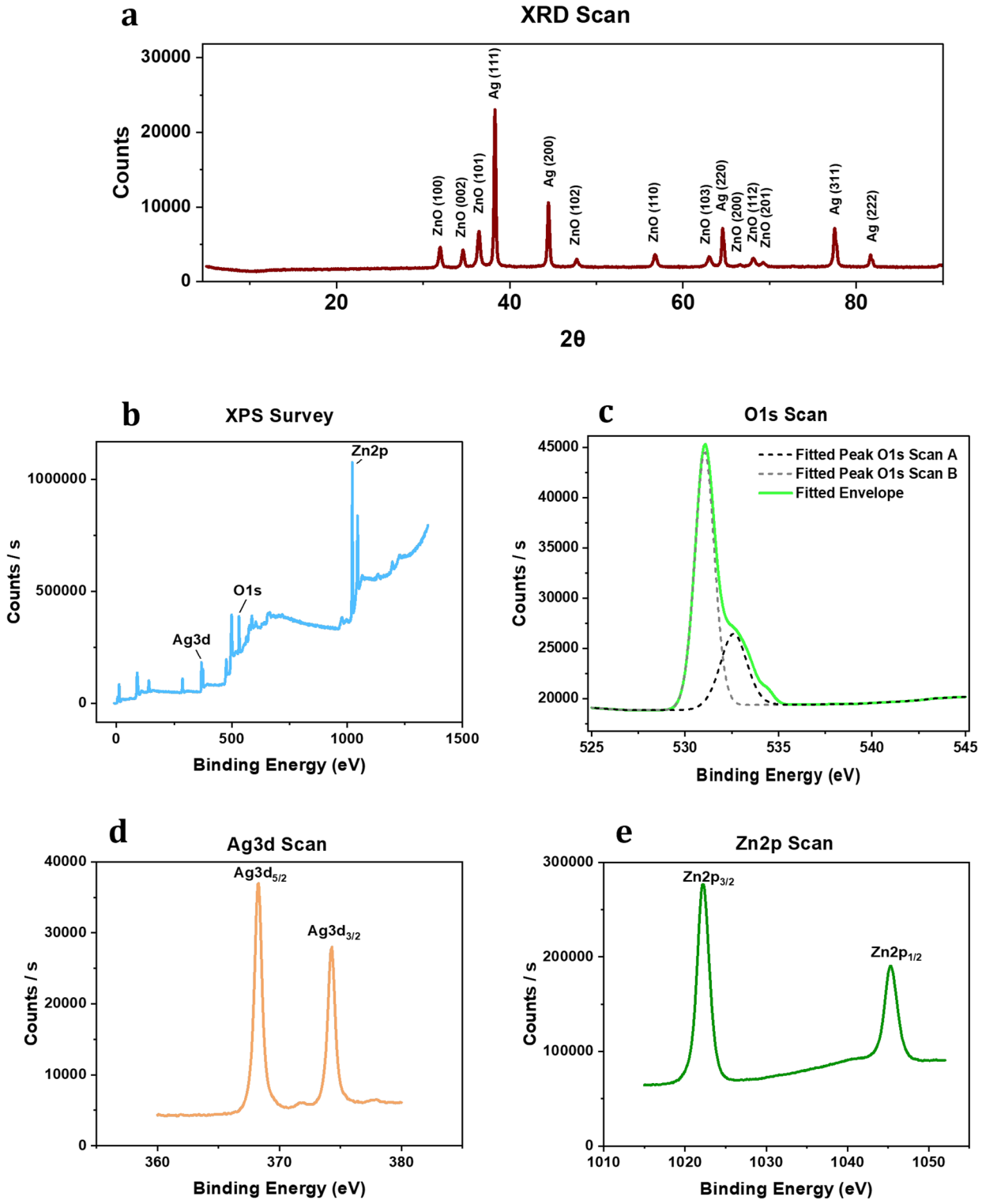

Fig. 1. Chemical Characterization of the ZnO–Ag nanocomposite. (**a**) XRD pattern (**b**) XPS survey scan (**c**) XPS scan of Ag (**d**) XPS scan of Zn (**e**) XPS scan of O.

topographical map, illustrated in Fig. 3c, uses shades of brown and yellow to depict the height variations across the surface, confirming the heterogeneous nature of the material. The height profile graph, Fig. 3b, provides detailed quantitative data of individual particles showing the average height of the of 20 nm.

Together, the AFM surface analysis highlights the potential of the synthesized material to mechanically disrupt bacterial cell membranes because of its sharp peaks. However, further investigation on the impact of the nanomterial length is needed to confirm the ability of these peaks to penetrate and disrupt bacteria. These

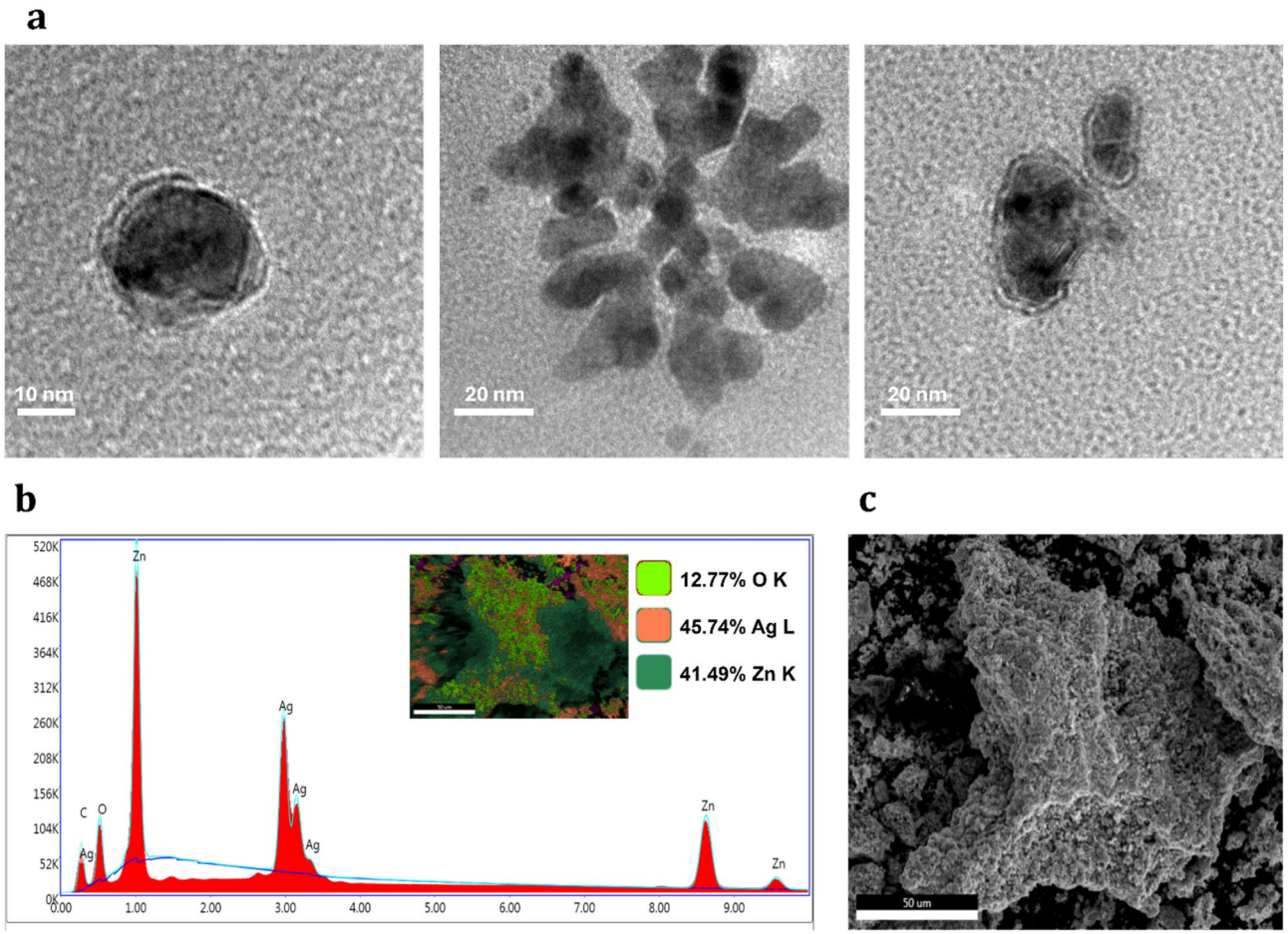

Fig. 2. TEM and SEM of ZnO–Ag nanocomposite. (**a**) TEM images of ZnO–AgNPs at 10 nm, 20 nm, showing spherical and aggregated morphologies. (**b**) EDX spectrum of the nanocomposite; the elemental mapping inset highlights the spatial distribution of Zn (green), Ag (orange), and O (bright green) (**c**) 50um SEM image of ZnO–AgNPs.

findings are crucial in understanding the antibacterial properties of the nanocomposite and its application in preventing biofilm-associated infections.

Electron paramagnetic resonance (EPR) analysis of the ZnO–Ag nanocomposite revealed the generation of reactive oxygen species (ROS), which play a critical role in its antibacterial efficacy. ROS are known to penetrate bacterial cell walls, inducing oxidative stress that damages cellular components and ultimately inhibits bacterial growth. The EPR spectra, presented in Fig. 4, highlight this phenomenon by comparing results under light irradiation and in the absence of light. Without light, no significant peaks were detected, indicating minimal ROS activity. However, upon light exposure, distinct signals corresponding to DMPO–CH_3 (or DMPO–CH_3) and DMPO–OOH adducts emerged, confirming the formation of methyl and superoxide radicals as summarized in Table 1.

The presence of the DMPO–OOH signal specifically indicates the production of superoxide radicals ($O_2^{\cdot-}$), which were trapped by DMPO[42]. These radicals likely form via photocatalytic processes, where the nanocomposite facilitates the reduction of molecular oxygen through a one-electron transfer mechanism. Upon excitation, the photocatalyst interacts with molecular oxygen, generating superoxide radicals, potent antimicrobial agents capable of inducing oxidative damage to bacterial cells[43].

Additionally, the detected DMPO–CH_3 signal suggests the formation of methyl radicals (CH_3), likely through hydrogen abstraction from methanol by reactive species such as superoxide radicals or other oxidants in the system[44,45]. Methanol itself does not produce EPR signals without radical formation, further substantiating this mechanism.

Interestingly, the absence of a DMPO–OH adduct, indicative of hydroxyl radicals ($OH^{\cdot}$), suggests that hydroxyl radicals are either produced at very low concentrations or react too rapidly to be trapped by DMPO. Due to their short lifetimes and high reactivity, hydroxyl radicals may have been consumed before detection through interactions with substrates like methanol[46]. Instead, the predominance of superoxide radicals, as suggested by the EPR spectra, underscores their key role in the antibacterial activity of the nanocomposite[42,47].

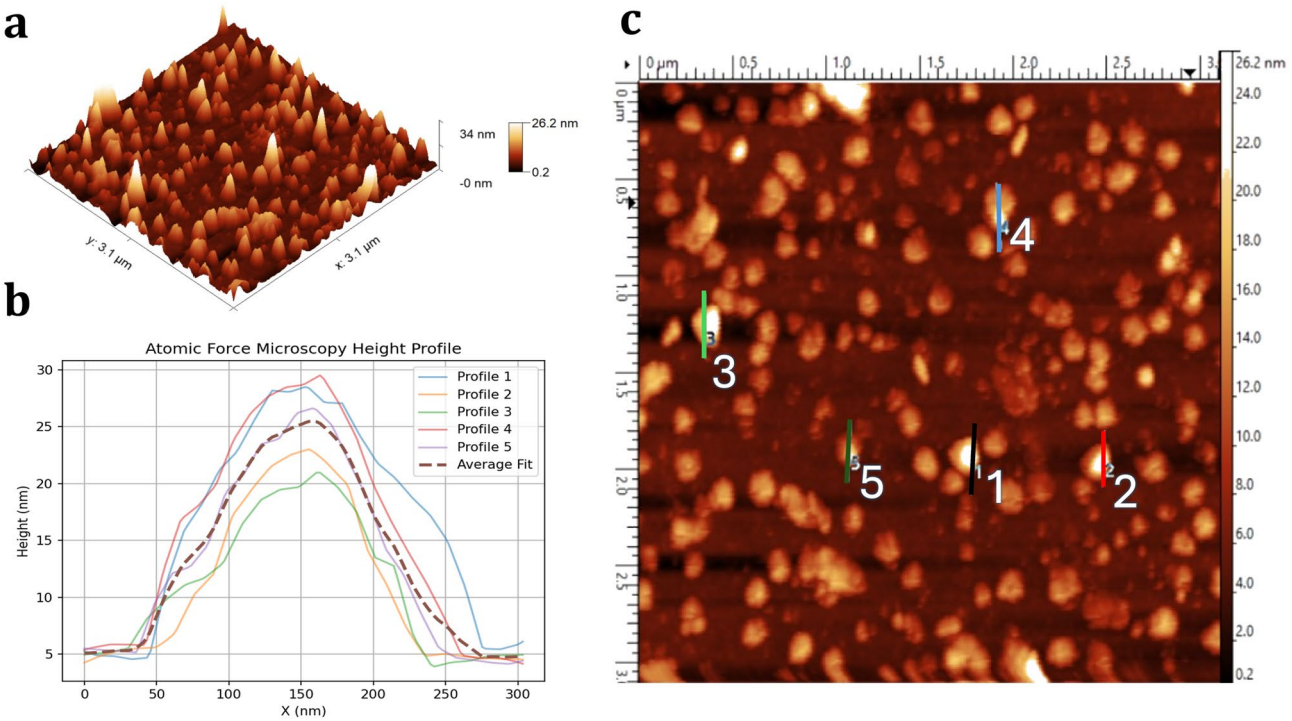

Fig. 3. AFM analysis of ZnO–Ag nanocomposite deposited on glass slide substrate. (**a**) 3D topographic representation showing nanoscale features with peak heights up to 34 nm. (**b**) 2D height map indicating the distribution of nanostructures across the scanned area. (**c**) Cross-sectional profiles indicating height of particles at different locations.

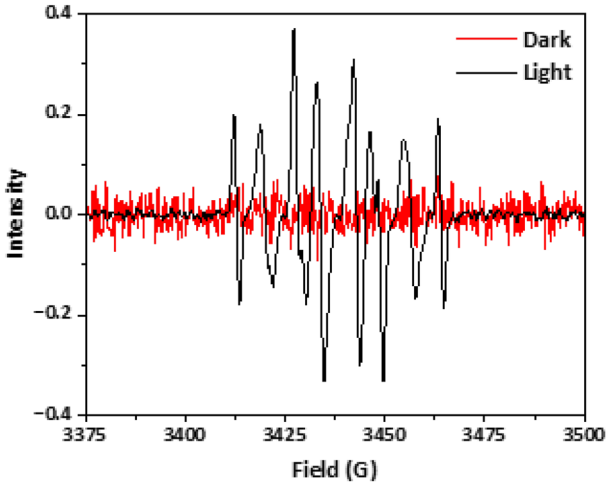

Fig. 4. EPR spectra of Ag–ZnO in the presence of DMPO and methanol, with and without light irradiation. "Light" indicates spectra recorded after 10 min of light irradiation prior to EPR measurement, while "Dark" refers to spectra recorded without any light exposure.

Adduct name	Spins/(mm^3)	M (spins)	Total spins
DMPO–CH_3	1.714e+13	2.845e−05	2.973e+14
DMPO–OOH	5.756e+13	9.559e−05	9.987e+14

Table 1. EPR-derived values for radical adducts under light irradiation.

Antibiofilm activity

To evaluate the antibiofilm properties of the synthesized nanocomposite, glass slides were coated with thenanocomposite. *P. aeruginosa*, was selected as a suitable model organism for this study due to its strong biofilm-forming ability and clinical relevance in biofilm-associated infections. After coating the glass slide, bacteria were subsequently added to assess their ability to form a biofilm. SEM images shown in Fig. 5 confirm that the bacteria could not form a biofilm on the coated samples, as shown in Fig. 5c, where the bacteria are sparsely distributed, forming only small aggregates limited to a single layer, without the surrounding biofilm matrix. In contrast, mature biofilm formation is evident on the uncoated samples shown in Fig. 5a, b where the entire surface area is covered with an aggregate of many bacterial layers, increasing the biofilm mass and surrounded by an extracellular polymeric matrix.

The suppression of biofilm formation on the coated slides is attributed primarily to the antimicrobial activity of the released Ag^{+} and Zn^{2+} ions, as well as the generation of ROS as confirmed in Fig. 4. The antibacterial activity of ZnO–Ag nanocomposites is driven by a multifaceted mechanism that combines the chemical and physical properties of both ZnO and Ag nanoparticles. Upon exposure to light, particularly UV irradiation, ZnO undergoes photocatalytic activation, generating reactive oxygen species (ROS) such as hydroxyl radicals (OH), superoxide anions (O_2^-), and singlet oxygen ($^1O_2$). These reactive species induce oxidative stress in bacterial cells, leading to DNA damage, thereby compromising cell viability[48]. Singh et al. demonstrated that ZnO nanoparticles can cause significant genotoxicity in *D. radiodurans*, as evidenced by DNA fragmentation observed through DAPI staining, with increased intracellular ROS generation implicated as a key driver of this damage[49].

Simultaneously, Ag nanoparticles release Ag^{+} ions that interact with vital cellular components, including thiol-containing enzymes and membrane proteins, leading to protein denaturation and disruption of essential metabolic pathways[17]. These ions can also penetrate the bacterial membrane, causing mitochondrial dysfunction and ribosomal disassembly, ultimately impairing protein synthesis and energy production[50]. Melo et al. confirmed that silver nanoparticles resulted in impairing *C. elegans* development and disrupting mitochondrial morphology and bioenergetics[51].

Additionally, AFM analysis shown in Fig. 3 confirmed the presence of nanoscale sharp features on the ZnO–Ag surface, which may contribute to physical stress or rupture of bacterial membranes upon contact.

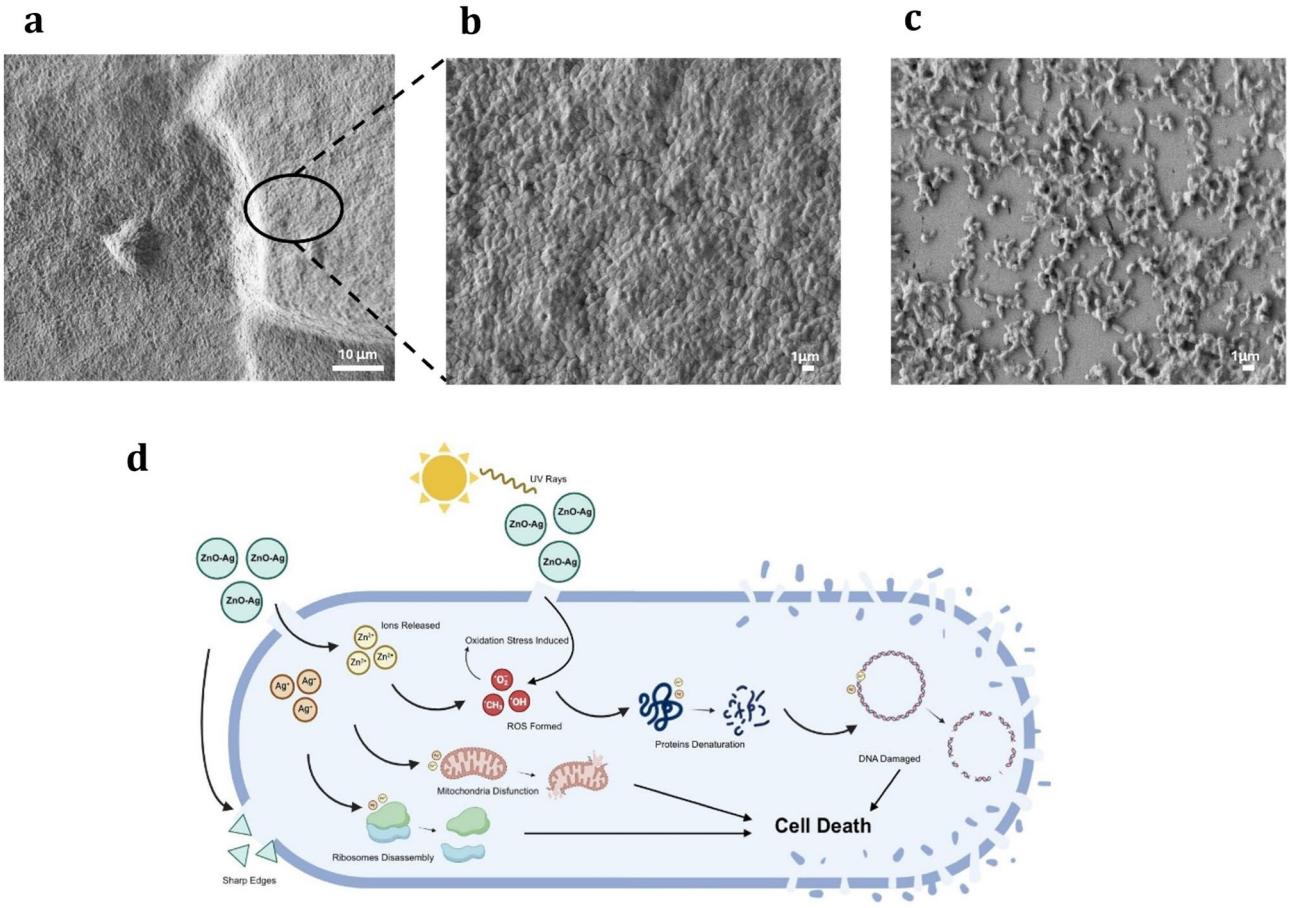

Fig. 5. SEM image for biofilm formation on (**a**) Non coated sample, where (**b**) shows biofilm surface structure on non-coated sample at higher magnification, and (**c**) Ag-ZnO coated sample. (**d**) Antibacterial mechanism of ZnO–Ag nanocomposites.

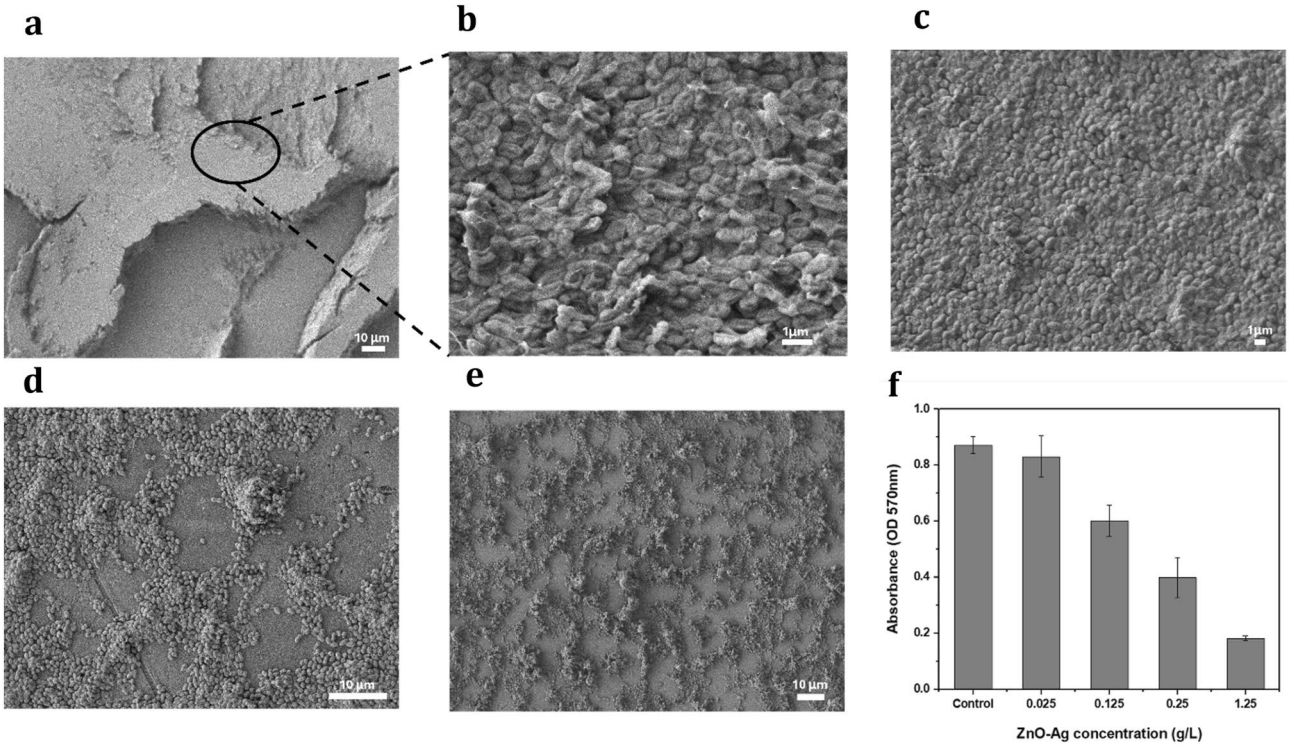

Fig. 6. Antibiofilm activity after adding varying concentrations of ZnO–Ag nanocomposite. Qualitative assessment of biofilm formation as shown in SEM images for ZnO–Ag concentrations of (**a**, **b**) 0.025 g/L, (**c**) 0.125 g/L, (**d**) 0.25 g/L, and (**e**) 1.25 g/L. (**f**) Quantitative assessment of biofilm formation using the crystal violet staining assay at each ZnO–Ag concentration.

While direct membrane disruption was not quantitatively assessed in this study, previous reports have shown that similar nanostructured surfaces with sharp features can mechanically compromise bacterial envelope integrity, enhancing antimicrobial efficacy[38]. Therefore, it is recognized as a possible secondary mechanism in preventing biofilm formation. This possible mechanism of actions of the NPs is visually summarized in Fig. 5d, which illustrates the sequential processes leading to bacterial cell death, including ROS generation, ion release, mitochondrial disruption, and potential DNA damage.

These results are promising for potential clinical applications, where coating medical devices with such a nanocomposite could prevent biofilm formation. Biofilms frequently develop on indwelling medical devices such as catheters, where they create a protective barrier that impedes antibiotic penetration, making treatment challenging once the biofilm is established[52]. Therefore, there is an urgent need to design catheters with surfaces that prevent bacterial adhesion to reduce the incidence of catheter-associated urinary tract infections (CAUTIs). Numerous studies have shown significant effectiveness in inhibiting biofilm growth of bacteria associated with urinary tract infections by coating the surface with silver nanoparticles[53]. However, despite these advances, no studies have specifically investigated the use of ZnO–Ag nanocomposites for this purpose, which could offer a novel and potent solution for biofilm prevention. While the current study utilized glass slides as a standardized model surface for initial evaluation, future work will be required to investigate its effectiveness on catheter materials and other clinically relevant substrates to fully assess its suitability for real-world biomedical applications. Additional research on the material is necessary to validate its clinical utility and address challenges associated with translating this technology into real-world applications.

To further validate the antibiofilm potential of the ZnO–Ag nanocomposite, biofilms were first grown and then treated with various concentrations of the nanocomposite. It can be observed that at lower concentrations of 0.025 g/L and 0.125 g/L, the nanocomposite did not significantly affect the biofilm, as shown in Fig. 6a–c. Figure 6b displays a clear biofilm matrix, characterized by a web-like structure surrounding the bacteria. In contrast, higher concentrations of the nanocomposite of 0.25 g/L and 1.25 g/L disrupted the biofilm structure, as seen in Fig. 6d–e, where bacterial cells are more dispersed. These findings were quantitatively confirmed by crystal violet staining, as shown in Fig. 6f. The amount of biofilm decreased as the concentration of the nanocomposite increased, indicated by a reduced absorbance at a wavelength of 570 nm.

In a study by Karthikeyan et al., approximately 100 µg/mL of pure AgNPs was required to highly inhibit *P. aeruginosa* biofilm formation[54]. In contrast, our ZnO–Ag nanocomposite achieved comparable antibiofilm activity at a total concentration of just 0.25 g/L. Given that the composite was synthesized using a 2:1 molar ratio of zinc acetate to silver nitrate, silver accounts for approximately one-third of the total nanocomposite mass. Therefore, at 0.25 g/L, the estimated Ag content is around 83 µg/mL, which is lower than the 100 µg/mL AgNP dose used in the previous study. This highlights the enhanced efficiency of the synthesized nanocomposite,

where silver's antimicrobial action is amplified through synergy with ZnO, enabling potent biofilm inhibition at reduced silver concentrations. Such reduced dosing also translates to lower cytotoxicity, supporting its suitability for biomedical applications.

On the other hand, pure ZnO often requires a somewhat higher threshold to achieve similar biofilm inhibition, whereas adding Ag enables strong effects at lower or equal concentrations. For example, undoped ZnO nanoparticles need 0.25–0.5 g/L to significantly reduce *P. aeruginosa* biofilms in some studies[55], whereas ZnO–Ag in this study achieved comparable or greater inhibition at 0.25 g/L. Furthermore, the concentration of 1.25 g/L, which effectively disrupted the biofilm structure in our experiments, is lower than the minimum biofilm inhibitory concentration (MBIC) of 1.875 ± 0.884 g/L reported in a study by Burlibaşa et al.[56], underscoring the potential of ZnO–Ag nanocomposites to inhibit biofilm formation at relatively lower concentrations and highlighting its enhanced efficiency.

The current results suggest that the nanocomposite could be an effective antibacterial agent for targeting established biofilms, particularly given the resilience of biofilms to traditional antibiotics due to their protective extracellular matrix[57]. However, further studies are needed to confirm the nanocomposite's efficacy against a wider range of bacterial strains and under diverse conditions to establish its broader applicability. Notably, compared to similar materials reported in the literature, this nanocomposite demonstrates significant antibiofilm activity at relatively lower concentrations, which could reduce cytotoxicity and enhance biocompatibility. Furthermore, the synthesis method employed is versatile, cost-effective, and scalable. These attributes, combined with its demonstrated antibiofilm properties, suggest that the ZnO–Ag nanocomposite could play a critical role in developing advanced coatings for medical devices.

Conclusion

In this study, we synthesized a ZnO–Ag nanocomposite using a simple and versatile dry chemical method and evaluated both its preventive and disruptive effects on *P. aeruginosa* biofilms. Comprehensive characterization confirmed the elemental composition and nanostructure of the material. Two antibacterial mechanisms were investigated based on existing literature: ROS generation and the presence of sharp edges. EPR analysis confirmed the presence of methyl and superoxide radicals, which interfere with bacterial metabolism and viability. Additionally, AFM imaging revealed nanoscale sharp edges, which may physically penetrate bacterial cell walls. The generation of these radicals is attributed to the synergistic effects of Ag and ZnO, while the sharp-edge morphology is attributed primarily to ZnO, as reported in previous studies. Future studies should focus on understanding the detailed molecular interactions between bacterial cells and the nanocomposite to further clarify the mechanistic pathways involved. Mechanistic studies employing advanced biochemical tools, such as real-time analysis of cell-nanoparticle interactions, could elucidate how direct contact initiates ROS release. Optimizing synthesis parameters could help fine-tune nanocomposite morphology for enhanced penetration into biofilms and bacterial membranes. SEM imaging confirmed that nanocomposite-coated surfaces inhibited biofilm formation and disrupted pre-formed biofilms, while crystal violet staining further validated the nanocomposite's concentration-dependent efficacy. Significantly reduced biofilm mass at concentrations ≥ 0.25 g/L, where the OD value based on crystal violet staining was less than 0.4. This concentration is notably lower than previously reported values, demonstrating the material's superior efficiency. Our findings highlight the potential of ZnO–Ag nanocomposites to prevent and treat biofilm-associated infections, offering a dual-action strategy applicable in both clinical and environmental contexts. The clear concentration-dependent response provides useful guidance for therapeutic dosing. Further evaluation of nanocomposite stability under different environmental conditions and against a broader range of microbial species and surfaces will be crucial for assessing its wider applicability. Surface functionalization or encapsulation strategies may also enhance targeted antimicrobial activity while minimizing cytotoxic effects. Moreover, ZnO–Ag nanocomposites represent a promising platform for antimicrobial coatings, combining ease of synthesis, scalability, and functional versatility, including the potential for co-delivery of additional agents.

Data availibility

The data that support the findings of this study are available from the corresponding author upon request.

Received: 17 February 2025; Accepted: 13 May 2025
Published online: 19 May 2025

References

1. GBD 2019 Antimicrobial Resistance Collaborators. Global mortality associated with 33 bacterial pathogens in 2019: A systematic analysis for the global burden of disease study 2019. *Lancet (London, England)* **400**(2221–2248), 2022. https://doi.org/10.1016/S0140-6736(22)02185-7 (2019).
2. Sharma, D., Misba, L. & Khan, A. Antibiotics versus biofilm: An emerging battleground in microbial communities. *Antimicrob. Resist. Infect. Control* **8**, 76. https://doi.org/10.1186/s13756-019-0533-3 (2019).
3. Sharma, S. et al. Microbial biofilm: A review on formation, infection, antibiotic resistance, control measures, and innovative treatment. *Microorganisms* **11**, 1614. https://doi.org/10.3390/microorganisms11061614 (2023).
4. Drenkard, E. Antimicrobial resistance of *Pseudomonas aeruginosa* biofilms. *Microbes Infect.* **5**, 1213–1219. https://doi.org/10.1016/j.micinf.2003.08.009 (2003).
5. Jamal, M. et al. Bacterial biofilm and associated infections. *J. Chin. Med. Assoc. JCMA* **81**, 7–11. https://doi.org/10.1016/j.jcma.2017.07.012 (2018).
6. Llor, C. & Bjerrum, L. Antimicrobial resistance: Risk associated with antibiotic overuse and initiatives to reduce the problem. *Ther. Adv. Drug Saf.* **5**, 229–241. https://doi.org/10.1177/2042098614554919 (2014).
7. Hetta, H. F. et al. Nanotechnology as a promising approach to combat multidrug resistant bacteria: A comprehensive review and future perspectives. *Biomedicines* **11**, 413. https://doi.org/10.3390/biomedicines11020413 (2023).

8. Zhang, S. et al. Antimicrobial properties of metal nanoparticles and their oxide materials and their applications in oral biology. *J. Nanomater.* **2022**, 2063265. https://doi.org/10.1155/2022/2063265 (2022).
9. Yougbaré, S. et al. Emerging trends in nanomaterials for antibacterial applications. *Int. J. Nanomed.* **16**, 5831–5867. https://doi.org/10.2147/IJN.S328767 (2021).
10. Nowak, M. & Barańska-Rybak, W. Nanomaterials as a successor of antibiotics in antibiotic-resistant, biofilm infected wounds?. *Antibiotics* **10**, 941. https://doi.org/10.3390/antibiotics10080941 (2021).
11. Tong, J. W. Case reports on the use of antimicrobial (silver impregnated) soft silicone foam dressing on infected diabetic foot ulcers. *Int. Wound J.* **6**, 275–284. https://doi.org/10.1111/j.1742-481X.2009.00610.x (2009).
12. Kim, Y.-T., Kim, K., Han, J. H. & Kimmel, R. M. Antimicrobial active packaging for food. In *Smart Packaging Technologies for Fast Moving Consumer Goods* (eds Kerry, J. & Butler, P.) (Wiley, New York, 2008). https://doi.org/10.1002/9780470753699.ch6.
13. Mendes, C. R. et al. Antibacterial action and target mechanisms of zinc oxide nanoparticles against bacterial pathogens. *Sci. Rep.* **12**, 2658. https://doi.org/10.1038/s41598-022-06746-4 (2022).
14. Quinteros, M., Cano-Aristizábal, V., Dalmasso, P., Paraje, M. & Páez, P. Oxidative stress generation of silver nanoparticles in three bacterial genera and its relationship with the antimicrobial activity. *Toxicol. In Vitro* **36**, 216–223. https://doi.org/10.1016/j.tiv.2016.08.007 (2016).
15. Singh, R., Cheng, S. & Singh, S. Oxidative stress-mediated genotoxic effect of zinc oxide nanoparticles on *Deinococcus radiodurans*. *3 Biotech* **10**, 66. https://doi.org/10.1007/s13205-020-2054-4 (2020).
16. Kalra, K., Chhabra, V. & Prasad, N. Antibacterial activities of zinc oxide nanoparticles: A mini review. *J. Phys. Conf. Ser.* **2267**, 012049. https://doi.org/10.1088/1742-6596/2267/1/012049 (2022).
17. Rodrigues, A. S. et al. Advances in silver nanoparticles: A comprehensive review on their potential as antimicrobial agents and their mechanisms of action elucidated by proteomics. *Front. Microbiol.* **15**, 1440065. https://doi.org/10.3389/fmicb.2024.1440065 (2024).
18. Godoy-Gallardo, M. et al. Antibacterial approaches in tissue engineering using metal ions and nanoparticles: From mechanisms to applications. *Bioact. Mater.* **6**, 4470–4490. https://doi.org/10.1016/j.bioactmat.2021.04.033 (2021).
19. Miškovská, A. et al. Antibiofilm activity of silver nanoparticles biosynthesized using viticultural waste. *PLoS ONE* **17**, 1–19. https://doi.org/10.1371/journal.pone.0272844 (2022).
20. Swidan, N. S., Hashem, Y. A., Elkhatib, W. F. & Yassien, M. A. Antibiofilm activity of green synthesized silver nanoparticles against biofilm associated enterococcal urinary pathogens. *Sci. Rep.* **12**, 3869. https://doi.org/10.1038/s41598-022-07831-y (2022).
21. Ashajyothi, C., Harish, K. H., Dubey, N. & Chandrakanth, R. K. Antibiofilm activity of biogenic copper and zinc oxide nanoparticles-antimicrobials collegiate against multiple drug resistant bacteria: a nanoscale approach. *J. Nanostruct. Chem.* **6**, 329–341. https://doi.org/10.1007/s40097-016-0205-2 (2016).
22. Agrawal, A. et al. Antibacterial and antibiofilm efficacy of green synthesized ZnO nanoparticles using *Saraca asoca* leaves. *Environ. Sci. Pollut. Res.* **30**, 86328–86337. https://doi.org/10.1007/s11356-023-28524-7 (2023).
23. García-Lara, B. et al. Inhibition of quorum-sensing-dependent virulence factors and biofilm formation of clinical and environmental *Pseudomonas aeruginosa* strains by zno nanoparticles. *Lett. Appl. Microbiol.* **61**, 299–305. https://doi.org/10.1111/lam.12456 (2015).
24. Gómez-Gómez, B. et al. Unravelling mechanisms of bacterial quorum sensing disruption by metal-based nanoparticles. *Sci. Total Environ.* **696**, 133869. https://doi.org/10.1016/j.scitotenv.2019.133869 (2019).
25. Huma, Z.-E. et al. Nanosilver mitigates biofilm formation via FapC amyloidosis inhibition. *Small* **16**, 1906674. https://doi.org/10.1002/smll.201906674 (2020).
26. Yarawsky, A. E., Johns, S. L., Schuck, P. & Herr, A. B. The biofilm adhesion protein Aap from staphylococcus epidermidis forms zinc-dependent amyloid fibers. *J. Biol. Chem.* **295**, 4411–4427. https://doi.org/10.1074/jbc.RA119.010874 (2020).
27. Al-Momani, H. et al. Anti-bacterial activity of green synthesised silver and zinc oxide nanoparticles against *Propionibacterium acnes*. *Pharmaceuticals* **17**, 255. https://doi.org/10.3390/ph17020255 (2024).
28. Siddiqi, K. S., Ur Rahman, A., Tajuddin, N. & Husen, A. Properties of zinc oxide nanoparticles and their activity against microbes. *Nanoscale Res. Lett.* **13**, 141. https://doi.org/10.1186/s11671-018-2532-3 (2018).
29. Dutta, G., Chinnaiyan, Sk., Sugumaran, A. & Narayanasamy, D. Sustainable bioactivity enhancement of ZnO–Ag nanoparticles in antimicrobial, antibiofilm, lung cancer, and photocatalytic applications. *RSC Adv.* **13**, 26663–26682. https://doi.org/10.1039/D3RA03736C (2023).
30. Shang, J., Sun, Y., Zhang, T., Liu, Z. & Zhang, H. Enhanced antibacterial activity of ag nanoparticle-decorated ZnO nanorod arrays. *J. Nanomater.* **2019**, 3281802. https://doi.org/10.1155/2019/3281802 (2019).
31. Rosenberg, M. et al. Selective antibiofilm properties and biocompatibility of nano-ZnO and nano-ZnO/Ag coated surfaces. *Sci. Rep.* **10**, 13478. https://doi.org/10.1038/s41598-020-70169-w (2020).
32. Suresh, P. et al. Antibiofilm, antibacterial and antioxidant activity of biofabricated bimetallic (Ag–ZnO) nanoparticles from elephantopus scaber l. *Biomass Convers. Biorefinery* **14**, 20911–20921. https://doi.org/10.1007/s13399-023-04230-9 (2024).
33. Arya, P. R. et al. Antioxidant, antibacterial and antibiofilm potential of green synthesized silver-zinc oxide nanocomposites from *Curcuma longa* extract against multi-drug-resistant enteroaggregative *E. coli*. *Med. Sci. Forum* **21**, 23. https://doi.org/10.3390/ECB2023-14088 (2023).
34. Shakerimoghaddam, A. et al. Evaluate the effect of zinc oxide and silver nanoparticles on biofilm and *icaA* gene expression in methicillin-resistant *Staphylococcus aureus* isolated from burn wound infection. *J. Burn Care Res.* **41**, 1253–1259. https://doi.org/10.1093/jbcr/iraa085 (2020).
35. Karthikeyan, A., Thirugnanasambantham, M. K., Khan, F. & Mani, A. K. Bacteria-inspired synthesis of silver-doped zinc oxide nanocomposites: A novel synergistic approach in controlling biofilm and quorum-sensing-regulated virulence factors in *Pseudomonas aeruginosa*. *Antibiotics* **14**, 59. https://doi.org/10.3390/antibiotics14010059 (2025).
36. Thaya, R. et al. Chitosan coated Ag/ZnO nanocomposite and their antibiofilm, antifungal and cytotoxic effects on murine macrophages. *Microb. Pathog.* **100**, 124–132. https://doi.org/10.1016/j.micpath.2016.09.010 (2016).
37. Alobaid, S. A. et al. Activity of silver-zinc nanozeolite-based antibiofilm wound dressings in an in vitro biofilm model and comparison with commercial dressings. *Discov. Nano* **20**, 26. https://doi.org/10.1186/s11671-025-04208-8 (2025).
38. Jeong, E. et al. Quantitative evaluation of the antibacterial factors of ZnO nanorod arrays under dark conditions: Physical and chemical effects on *Escherichia coli* inactivation. *Sci. Total Environ.* **712**, 136574. https://doi.org/10.1016/j.scitotenv.2020.136574 (2020).
39. Al-Gaashani, R. et al. Antimicrobial activity of ZnO–Ag–MWCNTS nanocomposites prepared by a simple impregnation-calcination method. *Sci. Rep.* **13**, 21418. https://doi.org/10.1038/s41598-023-48831-w (2023).
40. Wu, H.-Y. et al. Hierarchical Ag–ZnO microspheres with enhanced photocatalytic degradation activities. *Pol. J. Environ. Stud.* **26**, 871–880. https://doi.org/10.15244/pjoes/65363 (2017).
41. Fang, L. et al. Solvent polarity resulted in different structures and photocatalytic abilities of Ag/ZnO composites. *J. Sol-Gel Sci. Technol.* **93**, 695. https://doi.org/10.1007/s10971-019-05181-2 (2020).
42. Khachatryan, L. & Dellinger, B. Environmentally persistent free radicals (EPFRs)-2. are free hydroxyl radicals generated in aqueous solutions?. *Environ. Sci. Technol.* **45**, 9232–9239. https://doi.org/10.1021/es201702q (2011).
43. Wang, L., Fu, Y., Li, Q. & Wang, Z. Epr evidence for mechanistic diversity of cu(ii)/peroxygen oxidation systems by tracing the origin of dmpo spin adducts. *Environmental Science & Technology* **56**, 8796–8806. https://doi.org/10.1021/acs.est.2c00459 (2022).

44. Pei, S., You, S., Ma, J., Chen, X. & Ren, N. Electron spin resonance evidence for electro-generated hydroxyl radicals. *Environ. Sci. Technol.* **54**, 13333–13343. https://doi.org/10.1021/acs.est.0c05287 (2020).
45. Zhao, B., Ranguelova, K., Jiang, J. & Mason, R. P. Studies on the photosensitized reduction of resorufin and implications for the detection of oxidative stress with Amplex Red. *Free Radic. Biol. Med.* **51**, 153–159. https://doi.org/10.1016/j.freeradbiomed.2011.03.016 (2011).
46. Berczyński, P. et al. Free radical scavenging activity of novel thiazolidine-2,4-dione derivatives. *Luminescence* **28**, 900–904. https://doi.org/10.1002/bio.2454 (2012).
47. Murugesan, V., Hemann, C. & Zweier, J. L. Removal of H_2O2 and generation of superoxide radical: Role of cytochrome c and NADH. *Free Radic. Biol. Med.* **51**, 160–170. https://doi.org/10.1016/j.freeradbiomed.2011.04.007 (2011).
48. Dutta, R., Nenavathu, B. P., Gangishetty, M. K. & Reddy, A. Studies on antibacterial activity of ZnO nanoparticles by ROS induced lipid peroxidation. *Colloids Surf. B* **94**, 143–150. https://doi.org/10.1016/j.colsurfb.2012.01.046 (2012).
49. Singh, R., Cheng, S. & Singh, S. Oxidative stress-mediated genotoxic effect of zinc oxide nanoparticles on *Deinococcus radiodurans*. *3 Biotech* **10**, 66. https://doi.org/10.1007/s13205-020-2054-4 (2020).
50. Chauhan, A. et al. Photocatalytic dye degradation and antimicrobial activities of pure and Ag-doped ZnO using Cannabis sativa leaf extract. *Sci. Rep.* **10**, 7881. https://doi.org/10.1038/s41598-020-64419-0 (2020).
51. Mello, D. F. et al. In vivo effects of silver nanoparticles on development, behavior, and mitochondrial function are altered by genetic defects in mitochondrial dynamics. *Environ. Sci. Technol.* **56**, 1113–1124. https://doi.org/10.1021/acs.est.1c05915 (2022).
52. Gotlib, O. et al. Investigation of an improved electricidal coating for inhibiting biofilm formation on urinary catheters. *J. Mater. Res.* **10**, 339–348. https://doi.org/10.1016/j.jmrt.2020.11.089 (2021).
53. Pollini, M. et al. Antibacterial coatings on haemodialysis catheters by photochemical deposition of silver nanoparticles. *J. Mater. Sci. Mater. Med.* **22**, 2005–2012. https://doi.org/10.1007/s10856-011-4380-x (2011).
54. Karthikeyan, A., Thirugnanasambantham, M. K., Khan, F. & Mani, A. K. Bacteria-inspired synthesis of silver-doped zinc oxide nanocomposites: A novel synergistic approach in controlling biofilm and quorum-sensing-regulated virulence factors in *Pseudomonas aeruginosa*. *Antibiotics* **14**, 59. https://doi.org/10.3390/antibiotics14010059 (2025).
55. Elzahaby, D. A. et al. Inhibition of adherence and biofilm formation of *Pseudomonas aeruginosa* by immobilized ZnO nanoparticles on silicone urinary catheter grafted by gamma irradiation. *Microorganisms* **11**, 913. https://doi.org/10.3390/microorganisms11040913 (2023).
56. Burlibaşa, L. et al. Synthesis, physico-chemical characterization, antimicrobial activity and toxicological features of AgZnO nanoparticles. *Arab. J. Chem.* **13**, 4180–4197. https://doi.org/10.1016/j.arabjc.2019.06.015 (2020).
57. Sharma, D., Misba, L. & Khan, A. U. Antibiotics versus biofilm: An emerging battleground in microbial communities. *Antimicrob. Resist. Infect. Control* **8**, 76. https://doi.org/10.1186/s13756-019-0533-3 (2019).

Acknowledgements

The authors would like to express their sincere gratitude to the RICH (Research and Innovation Center on CO2 and Hydrogen), Khalifa University for their invaluable support in performing the EPR (Electron Paramagnetic Resonance) analysis. AN acknowledges funding from Khalifa University RIG-2023-005 and thanks Research and Innovation Center of Graphene and 2D Materials (RIC2D) for their support. AMP acknowledges funding from NIH-Al Jalila collaborative grant (AJF-NIH-19-KU) and Biotechnology Center, Khalifa University. AMP and DI acknowledge the financial support from FSU-2022-009 grant from Khalifa University.

Author contributions

F.A. and D.I.: conceptualized and designed the study, performed the experiments (F.A. performed material synthesis and characterization while D.I. performed antibiofilm activity experiments), collected the data and drafted the manuscript. S.A, L.N.: assisted in data collections and manuscript editing and revision. A.Z., A.R.: assisted in data collection and material-related experiments. A.F.Y., A.M.P, A.N: senior authors; provided feedback to experiments and the manuscript.

Declarations

Competing interests

The author declare no competing interests.

Additional information

Correspondence and requests for materials should be addressed to A.N.

Reprints and permissions information is available at www.nature.com/reprints.

Publisher's note Springer Nature remains neutral with regard to jurisdictional claims in published maps and institutional affiliations.